JPE 18-6-7

https://doi.org/10.6113/JPE.2018.18.6.1670
ISSN(Print): 1598-2092 / ISSN(Online): 2093-4718

Repetitive Control with Specific Harmonic Gain Compensation for Cascaded Inverters under Rectifier Loads

Zheng-Kai Lv*, Li Sun*, Jian-Dong Duan†, Bing Tian*, and HuiLing Qin**

†,*School of Electrical Engineering and Automation, Harbin Institute of Technology, Harbin, China
**No. 722 Research Institute of CSIC, Wuhan, China

Abstract

The further improvement of submarine propulsion is associated with the modularity of accumulator-fed inverters, such as cascaded inverters (CIs). CI technology guarantees smooth output voltages with reduced switch frequencies under linear loads. However, the output voltages of CIs are distorted under rectifier loads. This distortion requires harmonic suppression technology. One such technology is the repetitive controller (RC), which is commonly applied but suffers from poor performance in propulsion systems. In this study, the FFT spectrum of a CI under rectifier load is analyzed, and the harmonic contents are uneven in magnitude. For the purpose of harmonic suppression, the control gains at each harmonic frequency should be seriously considered. A RC with a specific harmonic gain compensation (SHGC) for CIs is proposed. This method provides additional control gains at low-order harmonic frequencies, which are difficult to achieve with conventional RCs. This SHGC consists of a band-pass filter (BPF) and proportional element and is easy to implement. These features make the proposed method suitable for submarine propulsion. Experimental results verify the feasibility of the improved RC.

Key words: Cascaded inverter (CI), Harmonic suppression, High-power rectifier load, Repetitive control (RC), Specific harmonic gain compensation (SHGC)

I. INTRODUCTION

Accumulator-fed inverters are widely used in various applications, such as submarine propulsion, where a battery management system (BMS) is necessary to balance the voltages among the accumulators. Many battery modules are connected in parallel and series to achieve high-power ratings. As a result, the complexity of BMSs increase considerably. Moreover, the accidental failures of individual battery modules disable the corresponding battery strings. In such a case, the operation of inverters is interrupted, and the available power ratings are restricted significantly. Consequently, the overall reliability of inverters decreases as the cascaded number of battery modules increases [1]-[3]. According to many experts, the evolution of accumulator-fed inverters involves the transition to modularity, reduced complexity of the BMS, and high reliability.

The technology of cascaded inverters (CIs) is a feasible option to promote this evolution. A CI is composed of several H-bridges in series connection, where the each H-bridge is fed by a battery string, the input voltage is considerably low, and the complexity of the BMS is reduced. In general, a CI can be divided into two types (i.e., single and three-phase CIs). Three-phase CIs can be considered as three independent single-phase CIs. Thus, the output voltage of each phase can be controlled separately. This feature enhances the adaptability of this type of CI to unbalanced loads. A CI has a high equivalent switching frequency, reduced switching loss, and low harmonic content. Therefore, the market of CIs continues to grow, expanding to their applications in battery energy storage systems. Aside from their high reliability and reduced complexity of the BMS, CIs achieve a desirable output voltage quality. Rectifier loads are one of the main loads for inverters used in submarine propulsion. The conventional control

Manuscript received Mar. 6, 2018; accepted Aug. 16, 2018
Recommended for publication by Associate Editor Kyo-Beum Lee.
†Corresponding Author: duanjiandong@hit.edu.cn
Tel: +86-18145148806, Harbin Institute of Technology, Harbin
*School of Electrical Eng. and Autom., Harbin Inst. of Technol., China
**No. 722 Research Institute of CSIC, China

© 2018 KIPE

method applied to linear loads is insufficient to maintain sinusoidal voltages under this condition. A highly desirable condition under rectifier load is one in which the inverter continues to maintain a good AC voltage quality.

The demands for harmonic suppression can be addressed by specific controllers that are simple and practical to use in submarine propulsion. Examples of such controllers include quasi-proportional resonant (QPR) and repetitive controllers (RCs). These methods are conventional harmonic suppression strategies and are based on the internal model principle [4]. The QPR controller is characterized by a simple configuration, low computational cost, and high DC voltage utilization [5]-[11]. Moreover, this controller is slightly suitable for the applications of three-phase independent control. RCs are preferred in harmonic suppression. In comparison with the conventional proportional–integral–derivative control, an RC guarantees a much higher gain at the fundamental frequency and its harmonics. In most existing studies, RCs were used to suppress periodic disturbances to ensure that the AC voltage meets national and international standards [12], [13]. [16], [17] proposed a high-order RC scheme that can reduce the partial derivative of an RC's control gains with an improved robustness. [18]-[22], [26]-[32] presented a dual-mode plug-in RC, a harmonic digital RC, a synchronous frame RC, a zero-phase-shift direct RC, and so on; good dynamic performance was reported. Although the aforementioned RCs improve the performance of inverters under rectifier loads, these control strategies are only appropriate for low power domains. In high-power domains, in which inverters operate under a relatively large dead time, a rectifier load is characterized by severe nonlinearities, which tend to degrade conventional harmonic suppression technology. Therefore, the control algorithm for submarine propulsion should preferably be simple and easy to implement.

In order to suppress the harmonic under high-power rectifier load, a RC with SHGC for CI is proposed for submarine propulsion application. This scheme is composed of an RC and SHGC. The SHGC consists of a BPF and proportional element. In this work, RCs for CIs are first introduced as a common harmonic suppression method. The output voltage total harmonic distortion (THD) under rectifier load is discussed, and the problems of a RCs are analyzed. This conventional method can eliminate high-order harmonics. However, low-order harmonics under this method remain large and thus dominate the THD. Suppressing these low-order harmonics further requires large control gains according to closed-loop control theory. For the above purposes, an improved RC with SHGC is proposed. This control scheme offers extra control gains for low-order harmonics, and the AC voltage quality can be improved prominently. Moreover, the proposed scheme is characterized by a simple configuration and excellent practicability, hence its suitability for submarine propulsion. The stability criteria

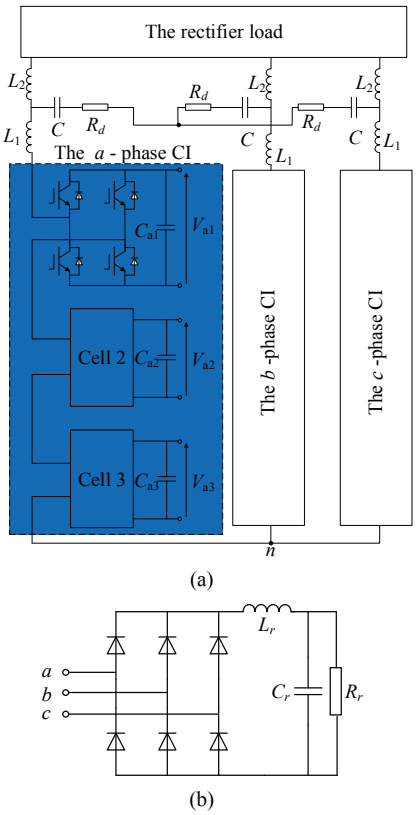

Fig. 1. Three-phase CI with a rectifier load: (a) Three-phase CI; (b) Rectifier load.

are derived for this improved RC, and advantages of the improved RC are confirmed by experimental results.

The remainder of this study is organized as follows. In Section II, the configuration of a CI and the drawbacks of RCs under rectifier loads are discussed. In Section III, an improved RC with SHGC is proposed, and the stability analysis is presented. In Section IV, a detailed controller design procedure is established. In Section V, the improved RC is applied to feed a high-power rectifier load. The experimental results verify the effectiveness of the proposed scheme. In Section VI, we conclude this study.

II. Problem with Rectifier Loads

A. CI Structure

Fig. 1 shows a three-phase CI, and Fig. 2 illustrates the block diagram of a control system. As a voltage source, the control loops of a CI are closed with respect to the AC voltages. In this study, the CI is composed of three single-phase CIs. Each single-phase CI consists of three cascaded H-bridges. The AC voltage of each phase is the summation of three H-bridges' outputs, and the voltage ripples can be reduced with the phase-shifted carrier pulse width modulation given by [25], which offers a high equivalent switching frequency. The outputs of the studied CIs can be controlled by three independent controllers. This feature decouples three-

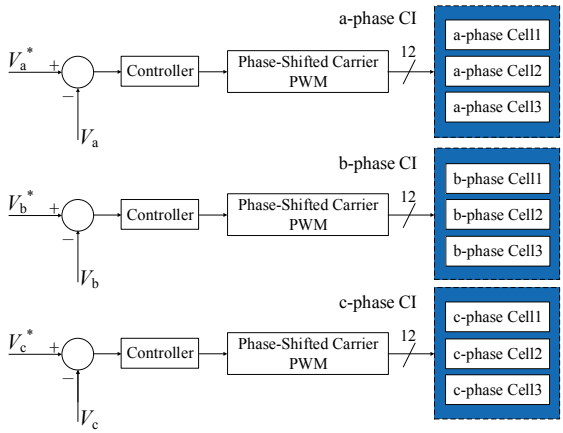

Fig. 2. Block diagram of the control system for CI.

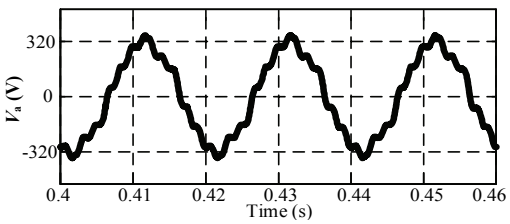

Fig. 3. Output voltage of CI.

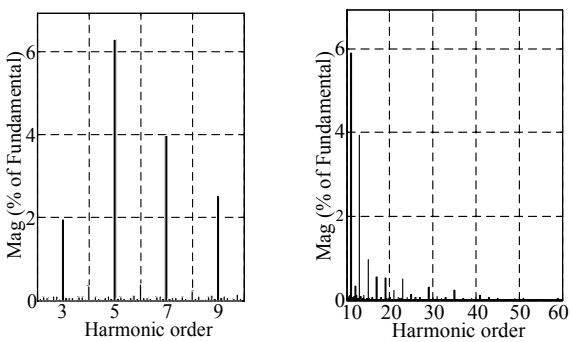

Fig. 4. Spectra of the output voltage: (a) Spectrum under the 10th order; (b) Spectrum over the 10th order.

phase load interactions and is appropriate under unbalanced load conditions. In this study, each single-phase CI is controlled by a QPR controller, and this method is preferred for linear load conditions. In submarine propulsion applications, the DC voltage source of a CI can be replaced by several individual cells, thereby resulting in a simple BMS. The working principle of a CI is detailed in [25] and is no longer discussed in this study. This study focuses on the harmonic suppression technologies under rectifier load conditions.

Rectifier load is common for submarine propulsion. The inverter used in submarine propulsion requires excellent adaptability to overload conditions, such as an AC current that is five times greater than that under rating condition and thus indicates a dead time that is too long to ensure a safe operation. As a result of these inherent nonlinearities, output

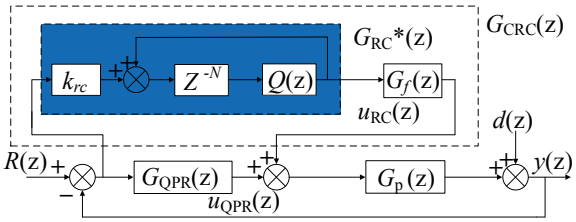

Fig. 5. Block diagram of the control system for CI.

voltages suffer from large harmonics. Fig. 3 shows the output of the CI under rectifier load; here, the dead time of inverters is set to 8.2 μs and is consistent with the experimental condition. Fig. 4 shows the spectrum of the output voltage.

As shown in Figs. 3 and 4, the THD is up to 10.93% when the CI operates under rectifier load. Notably, the CI is controlled by QPR controllers and suffers from severe harmonic pollution. The magnitudes of the 5th, 7th, and 11th harmonics are 6.2%, 3.95%, and 5.9%, respectively. These harmonic contents are uneven. The control gains for these harmonic contents should be infinite to suppress them. However, overly large control gains result in the instability of the control system. A practical approach is to set the values of these control gains such that they are unequal. Meanwhile, large harmonics are mainly located in the low-frequency domain under rectifier load. The harmonics over the 20th order have minor contributions to the THD. Therefore, the key point is to suppress the harmonics in the low-frequency domain to suppress the harmonic pollution introduced by the rectifier load.

Several methods have been proposed to attenuate voltage harmonics caused by rectifier loads. Among such methods, RCs have been identified as a feasible approach to improve AC voltage quality. An RC-controlled CI is discussed in the next section.

B. Conventional RC and Its Limitations

The structure of a conventional RC (CRC) is shown in Fig. 5. Such RC is realized on the basis of a QPR controller. In Fig. 5, the reference voltage signal is expressed as $R(z)$, the output signal is expressed as $y(z)$, and the objective plant is denoted by $G_p(z)$. Two filters $Q(z)$ and $G_f(z)$ are inserted into the CRC structure to optimize the robustness of the entire system. $G_{QPR}(z)$ and $G_{CRC}(z)$ are the transfer functions of the QPR controller and CRC, respectively. The QPR controller achieves the fast control of fundamental frequency, and the CRC ensures harmonic suppression.

Fig. 6 illustrates the bode plot of the CRC. As shown in the figure, the control gains at each harmonic frequency are slightly large. An excellent harmonic suppression can be achieved theoretically if harmonic frequencies are consistent with the resonant frequencies of the CRC.

The functionalities and limitations of the CRC are analyzed by the simulation results (Figs. 7 and 8). Fig. 7 shows the output of the CRC-controlled CI, and Fig. 8 presents the

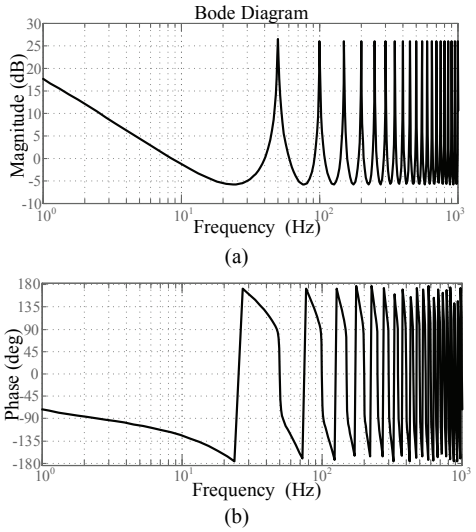

Fig. 6. Bode plot of the CRC: (a) Magnitude; (b) Phase.

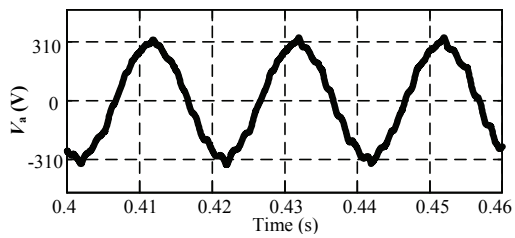

Fig. 7. Output voltage of parallel CRC-controlled CI.

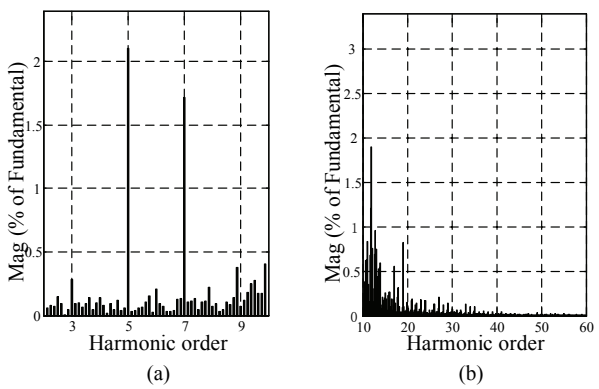

Fig. 8. Spectra of parallel CRC-controlled output voltage: (a) Spectrum under the 10th order; (b) Spectrum over the 10th order.

spectrum. Notably, the parameters in the simulation are similar to those in the experimental setup.

As shown in the figures, the THD of the output voltage is approximately 5.52% when the CI feeds a rectifier load. According to the comparison results of Figs. 8 and 3, the CRC achieves a satisfactory harmonic suppression performance. Hence, the CRC can improve the AC voltage quality. However, large harmonics exist in the AC voltage. According to Fig. 8, only high-order harmonics with magnitudes lower than 0.25% are suppressed, and they are unable to dominate the THD. Moreover, the magnitudes of the 5th and 7th harmonics are 2.1% and 1.7%, respectively. The low-order harmonics are still considerable and thus contribute greatly to the THD. Therefore, the CRC is unable to adequately suppress the low-frequency harmonic pollution caused by the rectifier load.

According to the abovementioned analysis, the CRC is insufficient to eliminate the low-order harmonics when the CI operates under rectifier load. The control gains for the harmonics should be set to large values to enhance the harmonic suppression performance. This approach can be achieved by increasing k_{rc} of the CRC, as shown in Fig. 5. Theoretically, a large k_{rc} of the CRC is always preferred for superior AC voltage quality. However, k_{rc} cannot be overly large because it could introduce and amplify a high-frequency interference that leads to the instability of the control system. However, if k_{rc} is not large enough, the low-order harmonics cannot be suppressed efficiently.

Therefore, the key point of this study is to increase control gains at low-order harmonics separately without influencing the high-order harmonic suppression performance. Moreover, the method should be simple and practical to be applicable to submarine propulsion.

III. IMPROVED RC

A. Structure of Improved RC

In this section, an improved RC is investigated to increase the control gains of the RC at low-order harmonics separately. Fig. 9 shows the structure of the improved RC, and Fig. 10 illustrates the detailed block diagram of the control system.

The difference between the improved RC and the CRC is the employment of SHGC. This SHGC plays a critical role in control gain amplification, as shown in Fig. 11. The SHGC consists of a BPF and proportional element K. The transfer function of SHGC can be expressed as follows:

$$G_{SHGC}(s) = K \cdot G_{BPF}(s), \tag{1}$$

where G_{BPF}(s) is the transfer function of the BPF and is expressed as follows:

$$G_{BPF}(s) = \frac{2\omega_{fc}s}{s^2 + 2\omega_{fc}s + \omega_{fr}^2}, \tag{2}$$

where ω_{fc} is the cutoff frequency of the BPF and ω_{fr} denotes the central frequency, which influences the control gain compensation for each harmonic.

The operation principle of SHGC is discussed as follows.

The low-order harmonic error should be separately magnified to increase the control gains. Therefore, the first step is to extract these low-order harmonics from the input error signal. Accordingly, a BPF is used for stated purposes. The central frequency of the BPF is set to the 5th order. The cutoff frequency is set to a value that guarantees that the low-order harmonics can be selected.

Aside from the extraction, the next important step is to

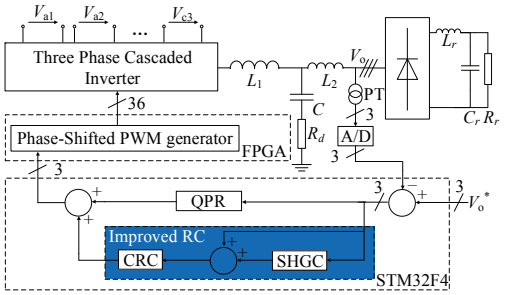

Fig. 9. Improved RC based on CI.

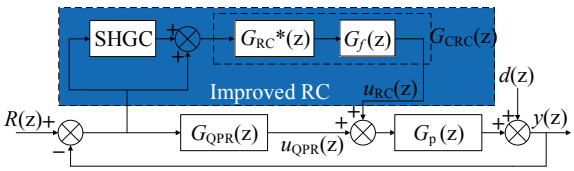

Fig. 10. Improved RC-managed closed-loop system.

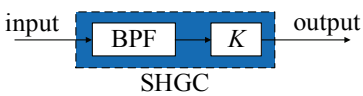

Fig. 11. Structure of SHGC.

TABLE I
PARAMETERS OF QPR CONTROLLER, CRC, AND IMPROVED RC

Controller	The quantity of parameters	Listed parameters
QPR	4	ω_c, ω_r, K_R, k_p
CRC	4	Q(z), k_{rc}, G_f(z), N
Improved RC	7	Q(z), k_{rc}, G_f(z), ω_{fc}, ω_{fr}, K, N

amplify these low-order harmonics. This approach can be achieved by multiplying a proportional element K with the extracted errors. This extracted error is superimposed over the initial one, thereby magnifying the specific harmonic error separately.

Finally, this synthetic error is transmitted into the CRC. This condition increases the control gains at low-order harmonics. Notably, the harmonic suppression performance for high-order harmonics is undegraded. According to closed-loop control theory, a large control gain always helps to reduce errors, indicating that low-order harmonics can be suppressed further. The parameters of the QPR controller, CRC, and improved RC are summarized on the basis of Eq. (6) and Figs. 5 and 10 (Table I). The QPR controller has the simplest configuration and lowest computational burden. However, the harmonic pollution introduced by the rectifier load is unsuppressed, as shown in Fig. 4. The CRC has an increasingly complex configuration, large calculation, and harmonic suppression capacity relative to the QPR controller. However, the CRC is unable to eliminate the low-frequency harmonics in the output, as shown in Fig. 8. Compared with the CRC shown in Fig. 5, the improved RC introduces SHGC, and only three additional parameters should be designed: the gain factor K, the cutoff frequency ω_{fc}, and the central frequency ω_{fr}. Moreover, the additional configuration and computational burden is not complex. Although the configuration of the improved RC is slightly more complex than those of the QPR controller and CRC, the low-frequency harmonics can almost be eliminated. Moreover, the improved RC can be paralleled with the QPR controller directly, and the parameters of the QPR controller need no alteration. Therefore, the proposed scheme is still simple and practical and a highly desirable method for submarine propulsion.

As shown in Fig. 5, G_{CRC}(z) can be expressed as

$$G_{CRC}(z)=G_f(z)G_{RC}^*(z)=G_f(z)\frac{k_{rc}z^{-N}Q(z)}{1-z^{-N}Q(z)}, \tag{3}$$

where N denotes the ratio of the sampling frequency and fundamental frequency and $G_f(z)$ is the stability filter, which can be expressed as follows:

$$G_f(z)=z^m S(z), \tag{4}$$

Where (3) indicates that the poles of the CRC are located at the fundamental frequency and its multiples. Q(z) can be a constant less than 1 or a low-pass filter to increase the system stability margin. The following Q(z) is selected due to its simple implementation:

$$Q(z)\le 0.99 \tag{5}$$

G_{QPR}(z) can be described in the s-domain as follows:

$$G_{QPR}(s)=k_p+\frac{\omega_c K_R s}{s^2+2\omega_c s+\omega_r^2}, \tag{6}$$

where ω_c determines the bandwidth of the QPR controller and ω_r is set to the fundamental frequency.

According to Fig. 10, the closed-loop transfer function for the improved RC can be derived as

$$\frac{y(z)}{R(z)}=\frac{\left(\left(1+G_{SHGC}(z)\right)G_{CRC}(z)+G_{QPR}(z)\right)G_p(z)}{1+\left(\left(1+G_{SHGC}(z)\right)G_{CRC}(z)+G_{QPR}(z)\right)G_p(z)}, \tag{7}$$

$$\frac{y(z)}{d(z)}=\frac{1}{1+\left(\left(1+G_{SHGC}(z)\right)G_{CRC}(z)+G_{QPR}(z)\right)G_p(z)}, \tag{8}$$

where Eq. (7) denotes the transfer function from the reference to the output and Eq. (8) is the transfer function from the disturbance to the output.

Figs. 12 and 13 show the bode plots of the BPF and improved RC. In comparison with those of the CRC, the control gains of the improved RC at low-order harmonics are enlarged by the inclusion of a SHGC. The control gains at fundamental and high-order harmonic frequencies are maintained to be equal to those in Fig. 6. Finally, by adjusting K of SHGC, all the harmonics and low-order harmonics are suppressed.

Remark 1. The main contribution of this study is the improved RC based on SHGC. SHGC is the harmonic compensator for low frequency harmonics that is unrealized

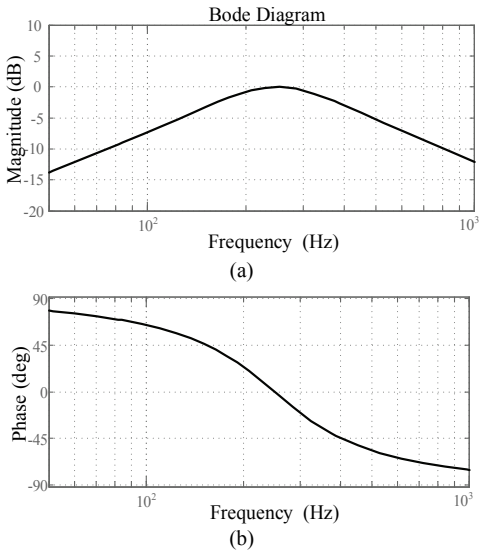

Fig. 12. Bode plot of the BPF.

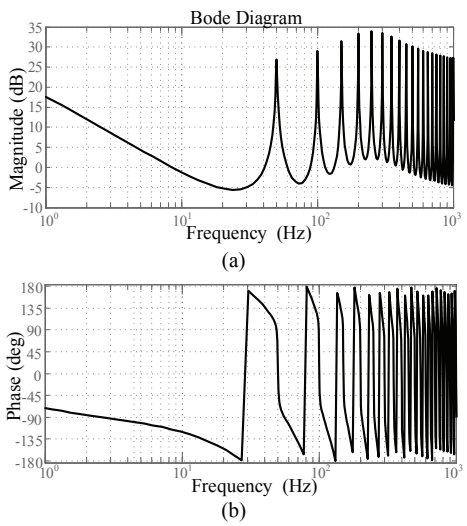

Fig. 13. Bode plot of the improved RC.

by the CRC. The low frequency harmonics are uncompensated for without SHGC. Thus, large low frequency harmonics will exist in the AC voltage. According to the aforementioned analysis, the harmonic pollution caused by the rectifier load is mainly located in the low frequency domain and contributes greatly to the THD. Therefore, the inadequate harmonic compensation will still result in an unsatisfactory AC voltage quality.

Remark 2. In this study, the improved RC is used to suppress the harmonic pollution in an islanded microgrid, whose control loop is closed by AC voltages. Fundamentally, the improved RC can be also used in grid-connected inverters with polluted or weak grids, whose control loop is closed by AC currents. The large harmonics of a grid can be selected, and their control gains are increased by setting ω_{fr} and ω_{fc} appropriately. This condition indicates that these harmonics can be suppressed further. Finally, the output current of the inverter is improved. The application of the improved RC in a grid-connected CI is part of our future work.

Remark 3. According to Table I, the improved RC has seven parameters: $Q(z)$, k_{rc}, $G_f(z)$, ω_{fc}, ω_{fr}, K, and N, where N denotes the number of samples of each cycle; $Q(z)$ and $G_f(z)$ are used to improve the stability of the proposed scheme; k_{rc} determines the control gains provided by the CRC; ω_{fc} and ω_{fr} dominate the compensation range of the SHGC; and K establishes the control gains provided by the SHGC. The detailed discussion of these parameters is presented in Section IV. Although the parameters of the improved RC are more than those of the CRC and QPR controller, the improved RC can achieve better harmonic performance than the CRC and QPR controller can. Moreover, the design procedure of the improved RC can be simplified significantly under the existing CRC and QPR controller; here, only three parameters of SHGC should be designed: ω_{fc}, ω_{fr}, and K. In this way, the improved RC is suitable to improve the performance of the CRC-controlled system.

B. Stability Analysis

According to Fig. 10, all poles of Eq. (9) must stay inside the unit circle when the CRC and SHGC are unplugged from the closed-loop system.

$$P_0(z)=\frac{P(z)}{1+G_{QPR}(z)P(z)} \tag{9}$$

On the basis of Eqs. (7) and (8), the characteristic polynomial of the improved RC can be expressed as

$$\begin{aligned}&1+[(1+G_{SHGC}(z))G_{CRC}(z)+G_{QPR}(z)]P(z)\\&=1+(1+G_{SHGC}(z))G_{CRC}(z)P(z)+G_{QPR}(z)P(z)\\&=(1+P(z)G_{QPR}(z))(1+\frac{(1+G_{SHGC}(z))G_{CRC}(z)P(z)}{1+P(z)G_{QPR}(z)})\\&=(1+P(z)G_{QPR}(z))(1+(1+G_{SHGC}(z))G_{CRC}(z)P_0(z)).\end{aligned} \tag{10}$$

As shown in Eq. (10), the improved RC becomes stable when the poles of Eq. (9) stay inside the unit circle and $1+(1+G_{SHGC}(z))G_{CRC}(z)P_0(z)\neq 0$ is met. The poles of Eq. (9) will be inside the unit circle by designing $G_{QPR}(z)$. Therefore, the following inequality should be true to guarantee the stability of the system:

$$\left|1+(1+G_{SHGC}(z))G_{CRC}(z)P_0(z)\right|\neq 0. \tag{11}$$

Substituting Eqs. (3) and (4) into Eq. (11) yields

$$\left|1-Q(z)z^{-N}+k_{rc}Q(z)z^{-N+m}S(z)(1+G_{SHGC}(z))P_0(z)\right|\neq 0. \tag{12}$$

If the following condition is met, Eq. (12) will be true:

$$\begin{aligned}&\left|Q(z)z^{-N}\left[1-k_{rc}z^{m}S(z)(1+G_{SHGC}(z))P_0(z)\right]\right|<1\\&\qquad\forall z=e^{j\omega},0<\omega<\pi.\end{aligned} \tag{13}$$

If the frequencies of $R(z)$ and $d(z)$ are located at $\omega_m=2\pi m/N$, with $m=0, 1, 2,\ldots, M$ ($M=N/2$ for even N and $M=(N-1)/2$ for odd N), then $z^N=1$ [30], Eq. (13) can

be simplified as

$$\left|Q(\mathrm{z})\left[1-k_{rc}\,\mathrm{z}^{m}\,S(\mathrm{z})(1+G_{SHGC}(\mathrm{z}))P_0(\mathrm{z})\right]\right|<1, z=e^{j\omega}. \quad (14)$$

Eq. (14) is rewritten as follows to facilitate the analysis:

$$\left|Q(\mathrm{z})\left[1-k_{rc}\,\mathrm{z}^{m}\,S(\mathrm{z})H(\mathrm{z})P_0(\mathrm{z})\right]\right|<1, z=e^{j\omega}, \quad (15)$$

where $H(\mathrm{z}) = 1 + G_{SHGC}(\mathrm{z})$.

Eq. (15) can be rewritten assuming that $H(\mathrm{z})$, $S(\mathrm{z})$, $P_0(\mathrm{z})$, and $Q(\mathrm{z})$ have magnitude and phase characteristics $N_H(e^{j\omega})$ and $\theta_H(e^{j\omega})$, $N_S(e^{j\omega})$ and $\theta_S(e^{j\omega})$, $N_{P0}(e^{j\omega})$ and $\theta_{P0}(e^{j\omega})$, and less than 1 and 0 repetitively, respectively.

$$\left|1-k_{rc}N_S(e^{j\omega})N_H(e^{j\omega})N_{P0}(e^{j\omega})\mathrm{e}^{-j\left[\theta_S(e^{j\omega})+\theta_H(e^{j\omega})+\theta_{P0}(e^{j\omega})+\mathrm{m}\omega\right]}\right|<1 \quad (16)$$

According to Euler's formula, considering that $k_{rc} > 0$, $N_H(e^{j\omega}) > 0$, $N_S(e^{j\omega}) > 0$, and $N_{P0}(e^{j\omega}) > 0$, we have

$$0<k_{rc}N_S(e^{j\omega})N_H(e^{j\omega})N_{P0}(e^{j\omega})<2\cos\left[\theta_S(e^{j\omega})+\theta_H(e^{j\omega})+\theta_{P0}(e^{j\omega})+\mathrm{m}\omega\right]. \quad (17)$$

The following condition must be satisfied to guarantee that Eq. (17) is true:

$$\left|\theta_S(e^{j\omega})+\theta_H(e^{j\omega})+\theta_{P0}(e^{j\omega})+\mathrm{m}\,\omega\right|<\frac{\pi}{2} \quad (18)$$

$$0<k_{rc}<\min\frac{2\cos\left[\theta_S(e^{j\omega})+\theta_H(e^{j\omega})+\theta_{P0}(e^{j\omega})+\mathrm{m}\,\omega\right]}{N_S(e^{j\omega})N_H(e^{j\omega})N_{P0}(e^{j\omega})}. \quad (19)$$

According to the abovementioned analysis, the phase compensator z^m can be designed by Eq. (18) in the stable RC system. The gain factor of the RC and SHGC can be selected by Eq. (19). Therefore, the improved RC is stable if the following conditions are satisfied.

(1) All the roots of $1+G_{QPR}(z)P(z)=0$ must stay in the unit circle.

(2) $\left|\theta_S(e^{j\omega})+\theta_H(e^{j\omega})+\theta_{P0}(e^{j\omega})+\mathrm{m}\,\omega\right|<\frac{\pi}{2}$

(3) $0<k_{rc}<\min\frac{2\cos\left[\theta_S(e^{j\omega})+\theta_H(e^{j\omega})+\theta_{P0}(e^{j\omega})+\mathrm{m}\,\omega\right]}{N_S(e^{j\omega})N_H(e^{j\omega})N_{P0}(e^{j\omega})}$

IV. Controller Design

A. Plant Modeling

Fig. 10 shows the control system of the improved RC, where L_1, L_2, and C are the parameters of the *LCL* filter. The passive damping resistor R_d is also used to suppress the resonance hazard of the *LCL* filter. Since the *LCL* filter is three order system and the L_2 is much smaller than L_1, and its influence on output voltage is negligible. In order to simplify the analysis. The transfer function of *LCL* filter can be simplified as

$$P(\mathrm{s})=\frac{n_1 s+n_0}{d_3 s^3+d_2 s^2+d_1 s+d_0}, \quad (20)$$

where $n_1 = R_dC$, $n_0 = 1$; $d_3 = 0$, $d_2 = L_1C$, $d_1 = R_dC$, and $d_0 = 1$. The parameters of the CI with the *LCL* filter are presented in Table II.

B. Design of the Proposed Control Scheme

The improved RC has several main parameters to be designed. These parameters can be summarized as follows.

(1) *QPR* controller, internal constant Q and N: According to the aforementioned analysis, the QPR controller should be designed to stabilize the control system when the improved RC is unplugged from the closed-loop system. The QPR controller can be designed according to engineering experience, which is no longer discussed in this study. Q is used to guarantee stability by decreasing the peak gain of the RC. In this study, $Q = 0.95$ is selected for ease of implementation. N denotes the ratio of sampling and fundamental frequencies. In this study, the sampling frequency is 5 kHz; therefore N is designed as 100.

(2) Band-pass filter $G_{BPF}(\mathrm{z})$: The BPF is used to extract specific harmonics from the input error signal. The selection of ω_{fr} determines which harmonic we want to suppress. Assuming that k_{rc} of the RC is constant, we enhance the control gain at the 5th harmonic when we set ω_{fr} such that it is five times that of the fundamental frequency. Similarly, the control gain at the 7th harmonic is enhanced when ω_{fr} is set to the 7th order. In this study, the 5th harmonic is slightly large in the output. Hence, the ω_{fr} is set to the 5th order. ω_{fc} is the cutoff frequency of the BPF and determines the range of the selected harmonics. The bode plots of $G_{BPF}(\mathrm{z})$ with different ω_{fc} are presented in Fig. 14. As shown in the figure, SHGC can select more harmonic contents with the increase of the ω_{fc}. According to Fig. 8, the output voltage is still polluted by large 5th- and 7th-order harmonics without SHGC. Therefore, the bandwidth of the BPF should be large so that the 5th and 7th harmonics can be selected. If the bandwidth of the BPF is too narrow, only the control gain at the 5th order can be compensated for efficiently, and the control gain compensation at the 7th order is insufficient. A possible way to settle this problem is to include another BPF for the 7th order in the SHGC. Although the BPF can magnify the control gain at the 7th order, it will increase the complexity of the SHGC further. A practical solution is to set the bandwidth of the BPF to a large value until it meets the control gain requirement for the 7th order. We should note that the bandwidth of the BPF cannot be overly large; otherwise, it will attenuate the rejection for high-order harmonics. In this study, $\omega_{fc} = 785$ rad/s is selected for the abovementioned purposes.

(3) Low-pass filter $S(\mathrm{z})$: $S(\mathrm{z})$ is a low-pass filter used to suppress high-frequency signals for stability. A Butterworth low-pass filter is preferred because of its fast attenuation characteristic after cutoff frequency, which can enhance the system stability. Therefore, a Butterworth low-pass filter, whose cutoff frequency is at 1 kHz, is used in this study. $S(\mathrm{z})$ can be expressed as follows:

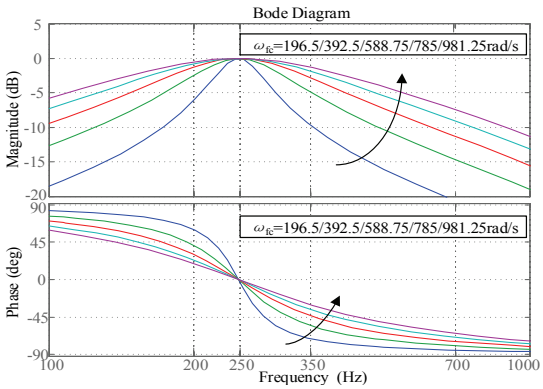

Fig. 14. Bode plots of $G_{BPF}(z)$ with different ω_{fc}.

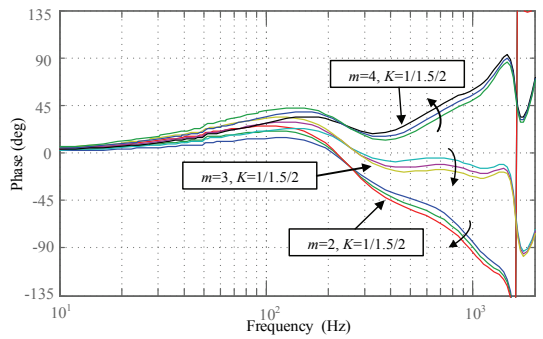

Fig. 15. $[\theta_S(e^{j\omega}) + \theta_H(e^{j\omega}) + \theta_{P0}(e^{j\omega}) + m\omega]$ with different m and K.

$$S(z) = \frac{0.004824z^4 + 0.1166z^3 + 0.2765z^2 + 0.1272z + 0.00961}{z^4 - 0.9889z^3 + 0.7287z^2 - 0.2457z + 0.03512}. \quad (21)$$

(4) Phase compensator z^m: z^m is a phase compensator used to offset the phase lag introduced by $G_{SHGC}(z)$, $P_0(z)$, and $S(z)$. Moreover, z^m can increase the phase margin to realize improved system stability, and a large k_{rc} can be chosen to increase the control gains of harmonics. A suitable m should be selected such that $[\theta_S(e^{j\omega}) + \theta_H(e^{j\omega}) + \theta_{P0}(e^{j\omega}) + m\omega]$ can approach zero to realize a desirable system stability. As noted from (1), (2), $H(z)$, and (16), the compensator gain K will also influence the value of $[\theta_S(e^{j\omega}) + \theta_H(e^{j\omega}) + \theta_{P0}(e^{j\omega}) + m\omega]$, and K should not be overly large; otherwise, overcompensation for the 5th and 7th harmonics will lead to system instability. Therefore, K should not be larger than 2. Fig. 15 illustrates $[\theta_S(e^{j\omega}) + \theta_H(e^{j\omega}) + \theta_{P0}(e^{j\omega}) + m\omega]$ with different m and K. As shown in Fig. 15, m has a much greater effect than K does in the frequency range greater than 200 Hz and less than 1 kHz. In this study, $m = 3$ is selected due to the minimum phase shift.

(5) Gain factor k_{rc} and K: According to Eq. (19), we can choose k_{rc} as

$$k_{rc} < \min \frac{2\cos\left(\theta_S(e^{j\omega}) + \theta_H(e^{j\omega}) + \theta_{P0}(e^{j\omega}) + m\omega\right)}{N_S(e^{j\omega})N_H(e^{j\omega})N_{P0}(e^{j\omega})} < \frac{2\cos\left[\max\left|\theta_S(e^{j\omega}) + \theta_H(e^{j\omega}) + \theta_{P0}(e^{j\omega}) + m\omega\right|\right]}{\max\left[N_S(e^{j\omega})N_H(e^{j\omega})N_{P0}(e^{j\omega})\right]}. \quad (22)$$

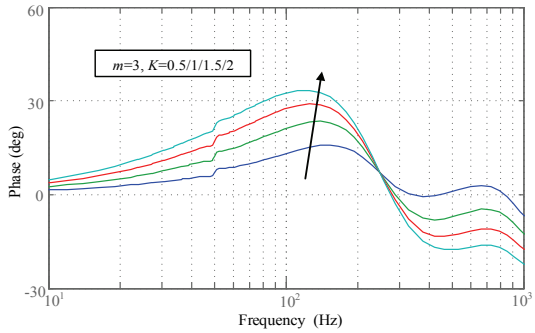

Fig. 16. $[\theta_S(e^{j\omega}) + \theta_H(e^{j\omega}) + \theta_{P0}(e^{j\omega}) + m\omega]$ with $m = 3$ and different K.

According to the aforementioned analysis, $m = 3$ is chosen. Fig. 16 illustrates $[\theta_S(e^{j\omega}) + \theta_H(e^{j\omega}) + \theta_{P0}(e^{j\omega}) + m\omega]$ with different K and $m = 3$ for the analysis of K's effect on the phase shift.

As shown in Fig. 16, $|\theta_S(e^{j\omega}) + \theta_H(e^{j\omega}) + \theta_{P0}(e^{j\omega}) + m\omega|$ becomes large with the increase of K. $K_{\max}$ is equal to 2 due to the design requirement. Therefore, the largest phase shift must exist when $m = 3$ and $K = 2$, and the following equation is true:

$$\max\left|\theta_S(e^{j\omega}) + \theta_H(e^{j\omega}) + \theta_{P0}(e^{j\omega}) + m\omega\right|_{m=3} = \max\left|\theta_S(e^{j\omega}) + \theta_H(e^{j\omega}) + \theta_{P0}(e^{j\omega}) + m\omega\right|_{m=3,K=2}. \quad (23)$$

In the figure, $\max|\theta_S(e^{j\omega}) + \theta_H(e^{j\omega}) + \theta_{P0}(e^{j\omega}) + m\omega|$ is 33.5°, with $K = 2$ in the frequency range less than 1 kHz. Therefore, the minimum numerator of Eq. (22) is equal to 1.668. If $K < 2$ is selected, the numerator of Eq. (22) must be greater than 1.668.

According to Eqs. (1), (2), (9), and (21), $N_H(e^{j\omega})$ is influenced by K, and $[N_S(e^{j\omega})\ N_{P0}(e^{j\omega})]$ is irrelevant to K. Consider the following inequality:

$$\max\left[N_S(e^{j\omega})N_H(e^{j\omega})N_{P0}(e^{j\omega})\right] \le \max\left[N_H(e^{j\omega})\right]\max\left[N_S(e^{j\omega})N_{P0}(e^{j\omega})\right]. \quad (24)$$

Therefore, Eq. (24) can be guaranteed if

$$k_{rc} = \frac{2\cos\left[\max\left|\theta_S(e^{j\omega}) + \theta_H(e^{j\omega}) + \theta_{P0}(e^{j\omega}) + m\omega\right|\right]}{\max\left[N_S(e^{j\omega})N_{P0}(e^{j\omega})\right]\max\left[N_H(e^{j\omega})\right]} = \frac{1.668}{\max\left[N_S(e^{j\omega})N_{P0}(e^{j\omega})\right]\max\left[N_H(e^{j\omega})\right]}. \quad (25)$$

According to Eq. (25), $\max[N_S(e^{j\omega})N_{P0}(e^{j\omega})]$ and $\max[N_H(e^{j\omega})]$ can be analyzed separately. Fig. 17 illustrates the curve of $[N_S(e^{j\omega})N_{P0}(e^{j\omega})]$.

As shown in Fig. 17, $[N_S(e^{j\omega})N_{P0}(e^{j\omega})]$ varies from 27.9 dB (0.04) to 31 dB (0.028) until 1 kHz. Thus, $\max[N_S(e^{j\omega})N_{P0}(e^{j\omega})]$ is 0.04. Substituting this value into Eq. (25) yields

$$k_{rc} = \frac{1.668}{0.04\max\left[N_H(e^{j\omega})\right]} = \frac{41.7}{\max\left[N_H(e^{j\omega})\right]}. \quad (26)$$

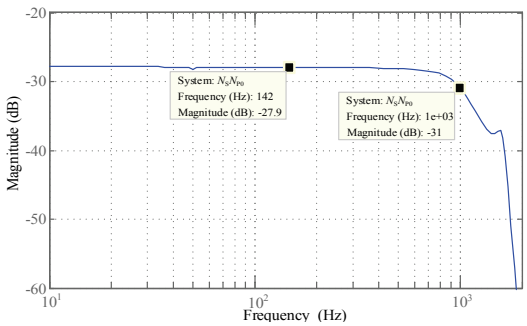

Fig. 17. Curve of $[N_S(e^{j\omega})N_{P0}(e^{j\omega})]$.

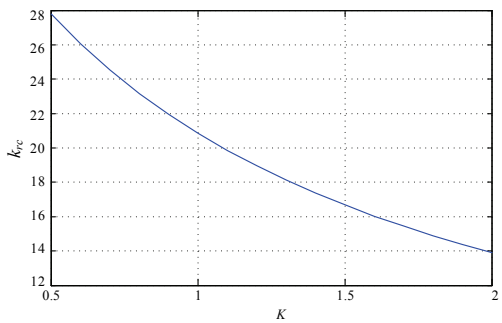

Fig. 18. Relationship between k_{rc} and K.

According to the expression of $H(z)$, the gain of unity is constantly equal to 0 dB, and $\max[N_H(e^{j\omega})]$ is determined by $G_{SHGC}(z)$, which can be equivalent to a superposition of the SHGC and unity. From the aforementioned analysis, SHGC consists of a BPF and proportional element K, and the BPF has the largest control gain at ω_{fr}. Therefore, $H(z)$ also has the largest control gain at ω_{fr}. Substituting $\omega = \omega_{fr}$ into $H(z)$ yields

$$\max\left[N_H(e^{j\omega})\right] = 1 + K \ . \tag{27}$$

Substituting Eq. (27) into Eq. (26), we have the relationship between k_{rc} and K, which is also plotted in Fig. 18.

$$k_{rc} = \frac{41.7}{1+K} \tag{28}$$

As shown in Fig. 18, k_{rc} and K cannot be designed separately because k_{rc} should be inversely proportional to K. Only $k_{rc} < 14$ can be chosen when $K = 2$ is selected; this case leads to the overcompensation of the 5th and 7th harmonics. Moreover, the control gains at the other harmonics will be inadequate. Thus, the overly large K is suppressed, which is consistent with the aforementioned analysis. However, an overly large k_{rc} is also suppressed because the immense control gains will reduce the stability margin of the system.

The model uncertainties of $P_0(z)$ also require close attention. According to Fig. 18, k_{rc} or K should be smaller than the theoretical value. In this study, we assume that the control system has 25% model uncertainties. k_{rc} and K are determined by the following inequality:

$$k_{rc} \le \frac{41.7 \times 0.75}{1+K} = \frac{31.275}{1+K} \ . \tag{29}$$

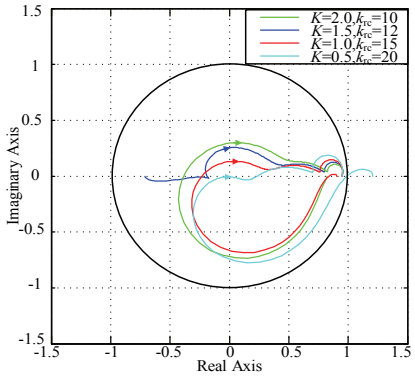

Fig. 19. Locus of $Y(e^{j\omega Ts})$ with different combinations of K and k_{rc}.

According to Eq. (29), the alternative design of K and k_{rc} can be summarized as follows:

(a) $K = 2$, $k_{rc} = 10$;

(b) $K = 1.5$, $k_{rc} = 12$;

(c) $K = 1$, $k_{rc} = 15$;

(d) $K = 0.5$, $k_{rc} = 20$.

Moreover, according to Eq. (15), assuming that $Y(e^{j\omega Ts}) = Q(e^{j\omega Ts})[1 - k_{rc}z^m H(e^{j\omega Ts})S(e^{j\omega Ts})P_0(e^{j\omega Ts})]$, the curve of $Y(e^{j\omega Ts})$ must stay inside the unity circle. We hope that $Y(e^{j\omega Ts})$ has a small magnitude, which indicates a large stability margin, fast error convergence, and excellent steady-state harmonic suppression [28], [29]. Fig. 19 illustrates the locus of $Y(e^{j\omega Ts})$ ($\omega \in [0, \pi / T_s]$) with different combinations of k_{rc} and K, where the T_s denotes the sampling period.

As shown in Fig. 19, the locus exceeds the unity circle due to the overly large control gains when $k_{rc} = 20$ and $K = 0.5$, which is consistent with the aforementioned analysis. The rest of the locus is located inside the unity circle. Moreover, the curve of $Y(e^{j\omega Ts})$ with $k_{rc} = 12$ and $K = 1.5$ has a more stable margin than those of the others. In this study, $k_{rc} = 12$ and $K = 1.5$ are adopted. Furthermore, $k_{rc} = 10$, $K = 2$, $k_{rc} = 15$, and $K = 1$ are tested in the experiment.

According to the abovementioned analysis, we can obtain suitable controller parameters, and the controller is implemented by STM32F407. The proposed control algorithm is based on the C language and compiled by MDK5. FPGA is also used to generate 36 IGBT gate signals to control the nine H-bridges.

V. Experimental Results

A three-phase CI under a rectifier load is studied to verify the effectiveness of the improved RC. It is then compared with the CRC, which is defined as Eq. (3) and uses no SHGC. The rectifier circuit includes a three-phase diode rectifier with an *LRC* load. The experimental conditions are presented in Table II.

Fig. 20 shows the phase "a" output voltage and its spectrum with the CRC. According to the spectrum, the THD of the output voltage is 5.82%, which exceeds the 5% restriction value of the IEEE 1547 standard. Notably, according to Fig. 20, the low-order harmonics are slightly large without SHGC,

TABLE II
RELEVANT PARAMETERS FOR CI

Meaning and symbol	Value
Cascaded number n	3
DC Voltage $V_{a1}…V_{c3}$	200V
Output filter inductance L_1	1.45mH
Output filter inductance L_2	0.1mH
Output filter capacitor C	100μf
Damping resistor R_d	1Ω
Rectifier Load L_r	100μH
Rectifier Load C_r	1900μf
Rectifier Load R_r	15Ω
Fundamental frequency f_0	50Hz
Sampling frequency f_s	5kHz
Switching frequency f_{sf}	5kHz
Amplitude of reference V_0^*	311V
Dead-time T_d	8.2μs

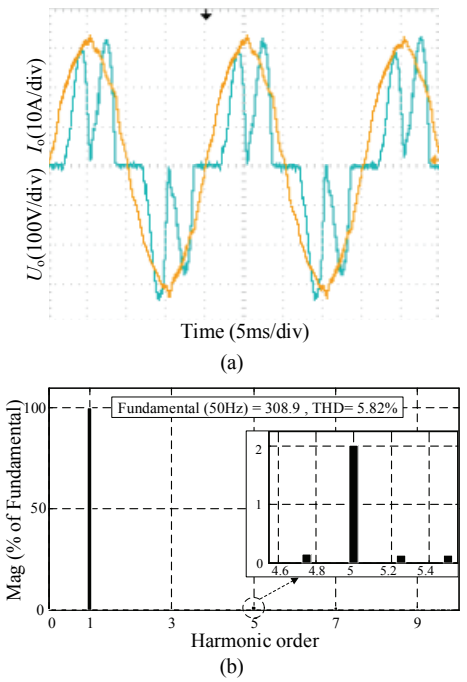

Fig. 20. Phase "a" voltage and spectrum under CRC: (a) Waveform; (b) Spectrum for phase "a" voltage.

and the maximum amplitudes of these harmonics is equal to 2%, which will still result in an unsatisfactory AC voltage quality. This condition is due to the weak control gains for these harmonics. Fundamentally, an overly large CRC gain factor is suppressed, thereby resulting in system instability. This problem can be settled by including a SHGC in the existing CRC. Such addition is the primary contribution of this study.

Figs. 21, 22, and 23 illustrate the phase "a" voltages and spectrum under the improved RC with different combinations of K and k_{rc}. The THD values of the output voltage in Figs. 21, 22, and 23 are only 2.66%, 2.63% and 2.65%, respectively,

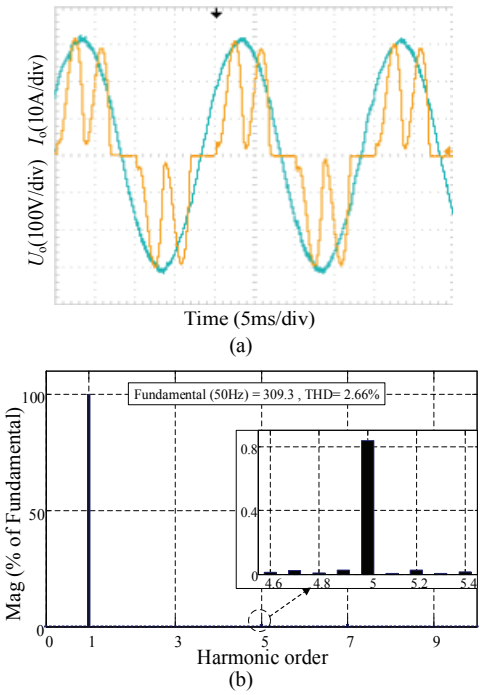

Fig. 21. Waveform and spectrum for the phase "a" voltage under the improved RC with $K = 1$ and $k_{rc} = 15$: (a) Waveform; (b) Spectrum for the phase "a" voltage.

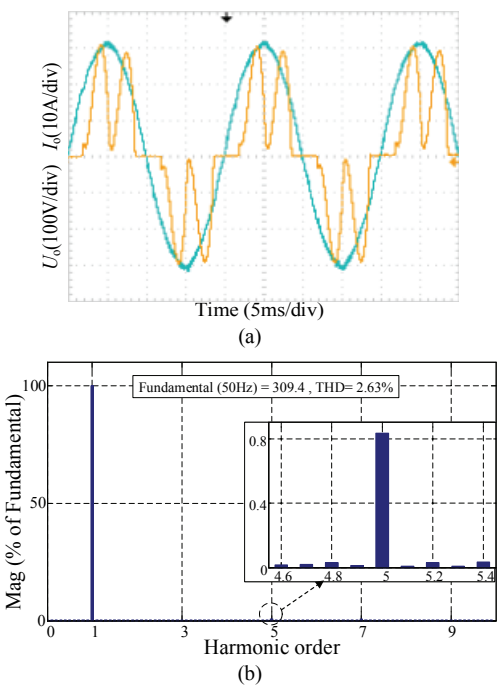

Fig. 22. Waveform and spectrum for the phase "a" voltage under the improved RC with $K = 1.5$ and $k_{rc} = 12$: (a) Waveform; (b) spectrum for the phase "a" voltage.

when SHGC is used. This result is much lower than that without SHGC. The low-frequency harmonics are compensated for significantly, and the maximum amplitudes of the low-order harmonics are approximately equal to 0.8%, which is much lower than that in Fig. 20. Therefore, the improved RC can

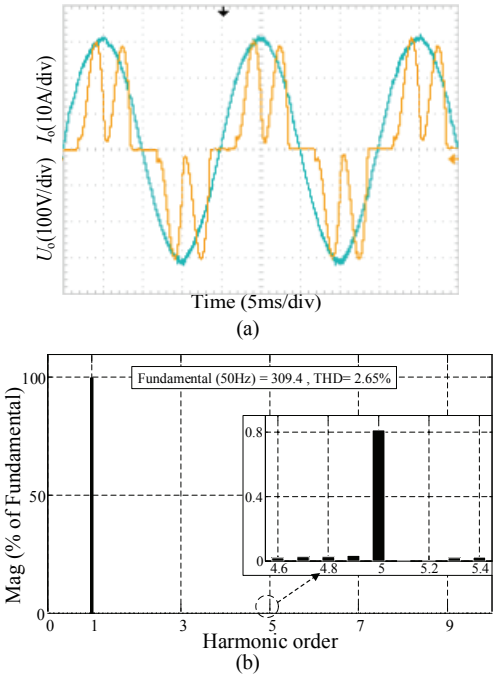

Fig. 23. Waveform and spectrum for the phase "a" voltage under the improved RC with $K = 2$ and $k_{rc} = 10$: (a) Waveform; (b) Spectrum for the phase "a" voltage.

suppress the low-order harmonics further relative to the CRC by compensating for the control gains of low-frequency harmonics. The result is a satisfactory AC voltage quality. Moreover, the THD of the output voltage is smaller than those of other two combinations of k_{rc} and K when $k_{rc} = 12$ and $K = 1.5$, which is consistent with the aforementioned analysis. Nevertheless, the improved RC is based on a particularly simple alteration on the existing CRC and can obtain strong harmonic suppression that is desirable in most applications.

The crest factor (CF) is used to describe the nonlinear distortion of an AC power waveform. CF is calculated by the ratio of the current peak to the current effective values. The optimal crest factor (OCF) desired by the load is this ratio when the input voltage is a pure sine wave. In general, most common electrical appliances are benefitted by a CF of 1.4, such as resistive load. However, nonlinear loads, such as rectifier loads, call for an OCF that is greater than 1.4 and approaches 2 or 3 [12], [13]. If the practical CF (PCF) is much lower than this OCF, the inverter is inefficient to supply the OCF desired by the load. Moreover, the output voltage waveform of the inverter will be distorted. Therefore, we hope that the PCF is close to the OCF. According to the MATLAB analysis, the OCF is calculated as 1.499 when $L_r = 2$ mH, $C_r = 1900$ μf, and $R_r = 15$ Ω are chosen. The OCF is calculated as 1.74 when $L_r = 1$ mH, $C_r = 1900$ μf, and $R_r = 15$ Ω are preferred. Moreover, the OCF is 2.6 when $L_r = 100$ μH, $C_r = 1900$ μf, and $R_r = 15$ Ω are selected. Figs. 24, 25, and 26 show the output voltage under the improved RC and CRC when the OCFs are 1.499, 1.74, and 2.6,

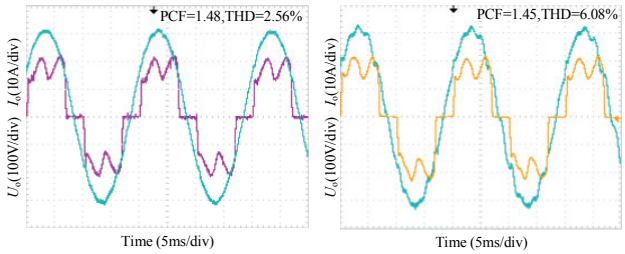

Fig. 24. Output voltage of the CI when the OCF is 1.499 under: (a) Improved RC; (b) CRC.

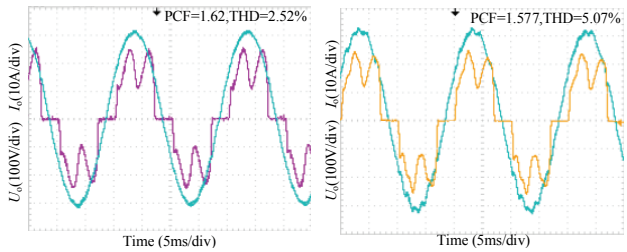

Fig. 25. Output voltage of CI when the OCF is 1.74 under: (a) Improved RC; (b) CRC.

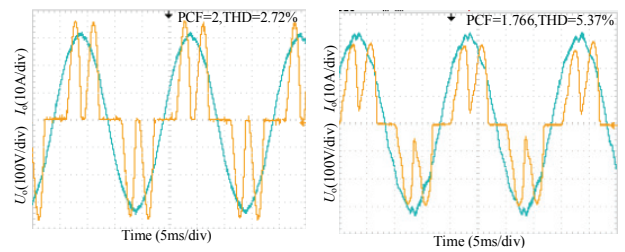

Fig. 26. Output voltage of CI when the OCF is 2.6 under: (a) Improved RC; (b) CRC.

respectively. As shown in Figs. 24, 25, and 26, the PCF is much lower than the OCF when SHGC is not utilized, and the CRC-controlled CI is unable to supply the OCF desired by the load. Thus, the output voltage is distorted and exceeds the 5% restriction value of the IEEE 1547 standard. The PCF is much closer to the OPF when SHGC is used, and the output voltage values are almost sinusoidal. The THD values are only 2.56%, 2.52%, and 2.72%, respectively, which are much lower than 5%. Therefore, the improved RC has much better adaptability to nonlinear loads than the CRC does.

Figs. 27 and 28 illustrate the THD of the output voltage under different C_r and L_r, respectively, to compare the adaptability of the improved RC and CRC to the detailed load parameters. In Fig. 27, $L_r = 0.1$ mH and $R_r = 15$ Ω are chosen. In Fig. 28, $C_r = 1900$ μF and $R_r = 15$ Ω are preferred. As shown in Figs. 27 and 28, the THD is constantly greater than 5% under different C_r and R_r when SHGC is not utilized. When SHGC is employed, the THD is almost constant and lower than 3% under different C_r and L_r; it is also much lower than that without SHGC. Therefore, compared with the CRC, the

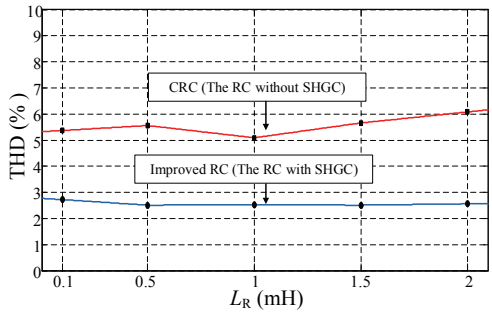

Fig. 27. THD of the output voltage under different C_r.

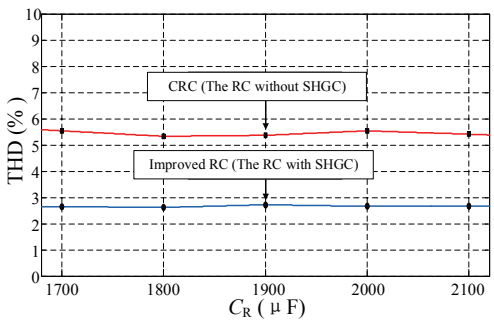

Fig. 28. THD of the output voltage under different L_r.

improved RC has stronger harmonic suppression capability and better adaptability to load parameters because of the utilization of SHGC.

VI. Conclusion

In this study, an RC with SHGC for CIs is proposed. The proposed RC features a simple configuration and is applicable to submarine propulsion applications. The improved RC compensates for control gains for the low-order harmonics introduced by rectifier loads. Hence, these harmonics are eliminated, and the AC voltage quality is significantly improved relative to the case involving the CRC. According to the experimental results, the improved RC achieves better AC voltage quality than the CRC does when feeding a high-power rectifier load. The THD of the AC voltage is approximately 2.63% with the improved RC, whereas this value is up to 5.82% with the CRC. Finally, the improved RC shows better adaptability to different rectifier load conditions than the CRC does.

References

[1] L. Maharjan, S. Inoue, H. Akagi, and J. Asakura, "State-of-charge (SOC)-balancing control of a battery energy storage system based on a cascadePWM converter," *IEEE Trans. Power Electron*., Vol. 24, No. 6, pp. 1628-1636, Jun. 2009.

[2] L. Maharjan, T. Yamagishi, H. Akagi, and J. Asakura, "Fault-tolerant operation of a battery-energy-storage system based on a multilevel cascade PWM converter with star configuration," *IEEE Trans. Power Electron*., Vol. 25, No. 9, pp. 2386-2396, Sep. 2010.

[3] L. Maharjan, T. Yamagishi, and H. Akagi, "Active-power control of individual converter cells for a battery energy storage system based on a multilevel cascade PWM converter," *IEEE Trans. Power Electron*., Vol. 27, No. 3, pp. 1099-1107, Mar. 2012.

[4] B. Francis and W. Wonham, "The internal model principle of control theory," *Automatica*, Vol. 12, No. 5, pp. 457-465, Sep. 1976

[5] D. N. Zmood and D. G. Holmes, "Stationary frame current regulation of PWM inverters with zero steady-state error," *IEEE Trans. Power Electron*., Vol. 18, No. 3, pp. 814-822, May 2003.

[6] R. Teodorescu, F. Blaabjerg, M. Liserre and P. C. Loh, "Proportional-resonant controllers and filters for grid-connected voltage-source converters," *IEE Proceedings-Electric Power Applications*, Vol. 153, No. 5, pp. 750-762, Sep. 2006.

[7] A. Kuperman, "Proportional-resonant current controllers design based on desired transient performance," *IEEE Trans. Power Electron*., Vol. 30, No. 10, pp. 5341-5345, Oct. 2015.

[8] G. Shen, X. Zhu, J. Zhang, and D. Xu, "A new feedback method for PR current control of LCL-filter-based grid-connected inverter," *IEEE Trans. Ind. Electron*., Vol. 57, No. 6, pp. 2033-2041, Jun. 2010.

[9] P. Mattavelli, "A closed-loop selective harmonic compensation for active filters," *IEEE Trans. Ind. Appl*., Vol. 37, No. 1, pp. 81-89, Jan./Feb. 2001.

[10] A. Timbus, M. Ciobotaru, R. Teodorescu, and F. Blaabjerg, "Adaptive resonant controller for grid-connected converters in distributed power generation systems," *Proc. 21st Annual IEEE Applications Power Electronics Conf*., pp. 1601-1606, 2006.

[11] R. Teodorescu, F. Blaabjerg, M. Liserre, and P. C. Loh, "Proportional-resonant controllers and filters for grid-connected voltage-source converters," *IEE Proceedings - Electric Power Applications*, Vol. 153, No. 5, pp. 750-762, Sep. 2006.

[12] H. R. Baghaee, M. Mirsalim, G. B. Gharehpetan, and H. A. Talebi, "Nonlinear load sharing and voltage compensation of microgrids based on harmonic power-flow calculations using radial basis function neural networks," *IEEE Syst. J.*, Vol. 12, No. 3, pp. 2749-2759, Sep. 2018.

[13] *IEEE Recommended Practices and Requirements for Harmonic Control in Electrical Power System*, IEEE Std. 519-1992, 1992.

[14] T. Hornik and Q. Zhong, "H∞ repetitive voltage control of gridconnected inverters with a frequency adaptive mechanism," *IET Power Electron*., Vol. 3, No. 6, pp. 925-935, Nov. 2010.

[15] T. Hornik and Q. Zhong, "A current-control strategy for voltage-source inverters in microgrids based on H∞ and repetitive control," *IEEE Trans. Power Electron*., Vol. 26, No. 3, pp. 943-952, Mar. 2011.

[16] M. Steinbuch, S. Weiland, and T. Singh, "Design of noise and period-time robust high-order repetitive control, with application to optical storage," *Automatica*, Vol. 43, No. 12, pp. 2086-2095, Dec. 2007.

[17] G. A. Ramos and R. Costa-Castello, "Power factor correction and harmonic compensation using second-order

-harmonic repetitive control," *IET Control Theory Appl.*, Vol. 6, No. 11, pp. 1633-1644, Jul. 2012.
[18] K. Zhou, D. Wang, B. Zhang, and Y. Wang, "Plug-in dual-mode structure repetitive controller for CVCF PWM inverters," *IEEE Trans. Ind. Electron.*, Vol. 56, No. 3, pp. 784-791, Mar. 2009.
[19] R. Costa-Castelló, R. Grinó, and E. Fossas, "Odd-harmonic digital repetitive control of a single-phase current active filter," *IEEE Trans. Power Electron.*, Vol. 19, No. 4, pp. 1060-1068, Jul. 2004.
[20] K. Zhou and D. Wang, "Zero tracking error controller for three-phase CVCF PWM inverter," *IEEE Trans. Power Electron.*, Vol. 36, No. 10, pp. 864-865, May 2002.
[21] S. Jiang, D. Cao, Y. Li, J. Liu, and F. Z. Peng, "Low-THD, fast-transient, cost-effective synchronous-frame repetitive controller for three-phase UPS inverters," *IEEE Trans. Power Electron.*, Vol. 27, No. 6, pp. 2994-3005, Jun. 2012.
[22] H. P. Michels and H. Grundling, "Design of plug-in repetitive controllers for single-phase PWM inverters," *39th IAS Annual Meeting: Industry Applications Conf.*, 2004.
[23] C. Cosner, G. Anwar, and M. Tomizuka, "Plug in repetitive control for industrial robotic manipulators," in *Proc. IEEE Int. Conf. Robot. Autom.*, pp. 1970-1975, 1990.
[24] L. Maharjan, T. Yamagishi, and H. Akagi, "Active-power control of individual converter cells for a battery energy storage system based on a multilevel cascade PWM converter," *IEEE Trans. Power Electron.*, Vol. 27, No. 3, pp. 1099-1107, Mar. 2012
[25] Y. Liang and C. O. Nwankpa, "A new type of STATCOM based on cascading voltage-source inverters with phase-shifted unipolar SPWM," *IEEE Trans. Ind. Appl.*, Vol. 35, No. 5, pp. 1118-1123, Sep./Oct. 1999.
[26] W. Lu, K. Zhou, and D. Wang, "General parallel structure digital repetitive control," *Int. J. Contr.*, Vol. 86, No. 1, pp. 70-83, 2013.
[27] T. Liu and D. Wang, "Parallel structure fractional repetitive control for PWM inverters," *IEEE Trans. Ind. Electron.*, Vol. 62, No. 8, pp. 5045-5054, Aug. 2015.
[28] L. He, K. Zhang, J. Xiong, and S. Fan, "A repetitive control scheme for harmonic suppression of circulating current in modular multilevel converters," *IEEE Trans. Power Electron.*, Vol. 30, No. 1, pp. 471-481, Jan. 2015.
[29] K. Zhang, Y. Kang, J. Xiong, and J. Chen, "Direct repetitive control of SPWM inverter for UPS purpose," *IEEE Trans. Power Electron.*, Vol. 18, No. 3, pp. 784-792, May 2003.
[30] B. Zhang, D. Wang, K. Zhou, and Y. Wang, "Linear phase lead compensation repetitive control of a CVCF PWM inverter," *IEEE Trans. Ind. Electron.*, Vol. 55, No. 4, pp. 1595-1602, Apr. 2008.
[31] A. Lidozzi, C. Ji, L. Solero, F. Crescimbini, and P. Zanchetta, "Load-adaptive zero-phase-shift direct repetitive control for stand-alone four-leg VSI," *IEEE Trans. Ind. Appl.*, Vol. 52, No. 6, pp. 4899-4908, Nov./Dec. 2016.
[32] A. Lidozzi, M. Di Benedetto, S. Bifaretti, L. Solero, and F. Crescimbini, "Resonant controllers with three degrees of freedom for AC power electronic converters," *IEEE Trans. Ind. Appl.*, Vol. 51, No. 6, pp. 4595-4604, Nov./Dec. 2015.

Zheng-Kai Lv received his B.S. degree in Computer Science and Technology from Dalian Maritime University, Dalian, China, in 2014. He acquired his M.S. degree in Electrical Engineering from Harbin Institute of Technology, Harbin, China, in 2016. He is currently working toward his Ph.D. degree in Electrical Engineering at Harbin Institute of Technology. His research interests include renewable energy applications and control of power electronic converters.

Li Sun (M'08) received his B.S., M.S., and Ph.D. degrees in Electrical Engineering from Harbin Institute of Technology, Harbin, China, in 1982, 1986, and 1991, respectively. Since 1986, he has been with the Department of Electrical Engineering, Harbin Institute of Technology, where he is currently a Professor of Electrical Engineering. His research interests include electric machines and drives, renewable energy, power electronics, and EMC.

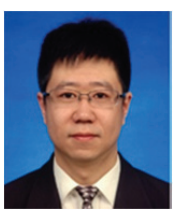

Jian-Dong Duan received his B.S. degree from Northeast Forestry University, Harbin, China, in 2007. He acquired the M.S. and Ph.D. degrees in Electrical Engineering from Harbin Institute of Technology, Harbin, China, in 2009 and 2014, respectively. He is currently with the Department of Electrical Engineering, Harbin Institute of Technology. His research interests include renewable energy and motor drives.

Bing Tian received his B.S. and M.S. degrees in Electrical Engineering from Harbin Engineering University, Harbin, China, in 2011 and 2013, respectively. He is currently working toward his Ph.D. degree in Electrical Engineering at Harbin Institute of Technology. His research interests include PM electric machines and drives and renewable energy.

HuiLing Qin received her B.S. degree in Measurement and Control Technology and Instrument from Wuhan University of Technology, Wuhan, China. She is currently with No. 722 Research Institute of CSIC. Her research interests include renewable energy and signal processing technology.